Determination of Rate Coefficients for Reactions of Formaldehyde Pyrolysis and Oxidation in the Gas Phase

B. Eiteneer, C.-L. Yu,† M. Goldenberg, and M. Frenklach*

Department of Mechanical Engineering, University of California, Berkeley, California 94720-1740

Received: February 19, 1998; In Final Form: April 28, 1998

Seven mixtures of formaldehyde and oxygen diluted in argon were studied behind reflected shock waves at temperatures from 1340 to 2270 K and pressures from 0.7 to 2.5 atm. Mixture compositions covered a range from pure pyrolysis to lean oxidation at a stoichiometric ratio of 0.17. The progress of reaction was monitored by laser absorption of CO molecules. Experimental rates of CO formation were found to be 80% higher, in the case of pyrolysis, and 30% lower, under lean oxidation, than those predicted by the current reaction model, GRI-Mech 1.2. The collected experimental data were subjected to extensive detailed chemical kinetics analysis, including optimization with the solution mapping technique. The analysis identified a strong correlation between two rate constants. Assuming a recent literature expression for one of them produced $k_{-1a} = 2.66 \times 10^{24} T^{-2.57} e^{-215/T}$ cm^6 mol^{-2} s^{-1} for the reaction H + HCO + M → CH_2O + M. A new expression was developed for the reaction $HO_2 + CH_2O \rightarrow HCO + H_2O_2$, $k_6 = 4.11 \times 10^4 T^{2.5} e^{-5136/T}$ cm^3 mol^{-1} s^{-1}, by fitting the present and literature results. With these modifications, the new reaction model provides good agreement with our experimental data and an acceptable agreement with most literature experimental observations.

Introduction

Reactions of formaldehyde molecules and formyl radicals play an important role in combustion chemistry. Formaldehyde has long been recognized as a critical kinetic intermediate in oxidation of hydrocarbon fuels,[1,2] especially methane[3] and methanol.[4] At the same time, the thermodynamic stability of formaldehyde results in its accumulation in concentrations large enough to cause environmental concerns.[5,6]

With the increasing demand for combustion models with predictive ability, there is a need for more accurate rate parameters. Several high-temperature kinetic studies were carried out in the past on formaldehyde pyrolysis[7−13] and oxidation.[14−20] All of them generally agree on the proposed reaction pathways, but the reported rate coefficients differ by as much as 1 order of magnitude. The likely cause of this disagreement is the inherent competition among elementary reactions, manifesting itself in correlations among the associated rate coefficients that precludes separate treatment.

We report here the results of a new experimental and modeling study of the formaldehyde reactions controlling its pyrolysis and oxidation at high temperatures. The numerical analysis is performed with an emphasis on identification of rate constant correlations.

Experimental Section

The experimental apparatus and procedures were the same as described in our previous studies.[21,22] Briefly, the experiments were performed in a conventional stainless steel double-diaphragm shock tube with an inner diameter of 8.26 cm, 1.5 m long driver section, and 4.9 m long driven section. Prior to each experiment, the test section of the shock tube was evacuated to at least 1×10^{-5} Torr. The combined leak-outgassing rate of the driven section was usually about 6×10^{-5} Torr min^{-1}. The shock tube was cleaned after each experiment. The progress of reaction was monitored behind reflected shock waves. The postshock conditions were calculated from the incident shock velocity assuming no chemical reaction and full vibrational relaxation.

The test mixtures were prepared manometrically, with a maximum uncertainty in the final reactant concentrations of less than 1%, and allowed to mix in a stainless steel tank for at least 24 h prior to experiments. Formaldehyde was produced by thermal dissociation of its trimer, 1,3,5-trioxane. Trioxane of purity higher than 99% was obtained from Aldrich. It was subjected to several trap-to-trap distillations and vacuum degassed prior to mixture preparation. The stated purities for the rest of the gases used in the present experiments were as follows: argon, 99.999% (Matheson); oxygen, 99.99% (MG Industries); carbon monoxide, 99.99% (Liquid Carbonic); helium, 99.999% (MG Industries). These gases were used without further purification.

The shock-tube apparatus is equipped with laser diagnostics for monitoring both OH and CO.[21,22] However, initial numerical tests and sensitivity analyses showed that measuring the concentration of OH in addition to that of CO does not add significantly more information, and hence only CO was monitored in the present study.

The concentration of CO was determined by resonance laser absorption.[22] A continuous-wave CO laser was operated at the 2 → 1 P(10) CO transition (2077.1 cm^{-1}). The intensity of the transmitted laser beam was collected at 1 μs intervals with the overall time constant of the electrooptical equipment of 0.6 μs. Absolute CO concentrations were determined using the Beer−Lambert law with the collision broadening half-width parameter 4.8×10^{-2} atm^{-1} cm^{-1} obtained earlier in our laboratory from CO calibration measurements.[22]

† Current address: Department of Chemistry, Cornell University, Ithaca, NY 14853.

S1089-5639(98)01184-0 CCC: $15.00
Published on Web 06/17/1998

TABLE 1: Experimental Conditions and Results

exptl run	T_5 (K)	T_0[a] (K)	C_0[b] (mol m^{-3})	$t_{0.25}$ (μs)	$t_{0.50}$ (μs)	$t_{0.75}$ (μs)	exptl run	T_5 (K)	T_0[a] (K)	C_0[b] (mol m^{-3})	$t_{0.25}$ (μs)	$t_{0.50}$ (μs)	$t_{0.75}$ (μs)
Series A: 1.97% CH_2O−Ar													
1	1639	1587	10.59	149.4	249.5	376.2	9	1862	1815	10.67	32.4	52.6	84.9
2	1656	1604	16.13	94.4	169.1	293.6	10	1876	1829	10.46	28.4	46.1	75.4
3	1701	1650	7.85	109.3	187.5	295.5	11	1934	1889	7.50	21.8	35.3	56.9
4	1750	1701	10.66	63.1	105.3	156.2	12	1936	1891	7.94	28.8	45.0	69.9
5	1760	1711	7.85	66.7	110.9	183.1	13	1992	1948	10.98	13.2	23.3	36.0
6	1826	1778	7.92	42.5	68.7	107.7	14	2003	1959	7.93	13.7	23.1	36.1
7	1840	1793	7.93	46.6	80.1	125.2	15	2011	1968	10.82	8.1	14.9	25.6
8	1856	1809	10.92	29.4	45.8	71.7							
Series B: 1.46% CH_2O−Ar													
16	1601	1561	15.8	132.2	221.8	348.7	21	1882	1847	8.05	34.6	57.4	88.1
17	1735	1697	6.73	122.0	198.1	304.4	22	2142	2111	6.69	9.3	15.3	24.5
18	1758	1721	16.62	36.2	61.2	93.8	23	2149	2118	6.70	7.0	13.6	21.9
19	1764	1727	6.75	104.2	166.9	255.6	24	2154	2124	6.71	7.2	14.9	22.4
20	1876	1841	16.62	19.9	33.3	54.1	25	2304	2276	8.53	2.7	5.6	10.5
Series C: 1.47% CH_2O−0.25% O_2−Ar													
26	1570	1529	16.13	87.8	122.1	159.9	32	1819	1783	6.32	50.0	69.8	90.3
27	1572	1531	10.76	121.8	164.7	211.8	33	1820	1784	15.76	19.3	29.8	40.5
28	1589	1549	15.75	92.5	129.2	169.4	34	1923	1888	6.34	34.5	49.2	66.1
29	1657	1618	10.76	83.0	113.4	146.4	35	1989	1956	6.33	22.6	33.0	43.9
30	1670	1631	15.88	54.6	72.9	92.3	36	2007	1974	6.25	17.9	25.7	35.4
31	1762	1725	16.01	28.8	42.0	56.1							
Series D: 1.00% CH_2O−0.60% O_2−Ar													
37	1370	1340	16.16	297.0	390.2	470.0	47	1615	1588	10.64	73.5	93.8	111.3
38	1412	1382	16.24	200.7	271.4	343.9	48	1688	1661	6.57	97.0	119.0	138.7
39	1447	1418	16.24	146.6	182.6	218.7	49	1701	1675	10.70	50.5	63.0	74.3
40	1451	1422	10.82	213.4	268.8	314.5	50	1720	1697	6.43	80.2	101.5	120.2
41	1485	1456	10.72	157.5	199.7	238.1	51	1743	1719	16.13	39.5	52.4	64.6
42	1497	1468	16.04	117.3	142.8	168.6	52	1785	1760	6.34	63.0	78.3	94.8
43	1568	1540	10.73	111.3	139.2	165.7	53	1828	1803	10.73	30.9	37.0	43.3
44	1574	1546	16.19	85.6	105.3	122.8	54	1837	1812	6.32	44.4	59.4	72.9
45	1585	1557	15.76	74.2	89.6	105.6	55	1900	1876	6.40	33.0	43.1	53.5
46	1614	1587	16.06	50.3	66.7	79.4							
Series E: 1.50% CH_2O−1.50% O_2−Ar													
56	1382	1338	10.85	293.7	341.6	384.8	65	1638	1598	10.74	44.0	55.4	64.4
57	1428	1385	15.93	124.3	152.8	175.1	66	1689	1650	6.29	72.0	87.2	101.3
58	1436	1393	10.72	170.9	210.5	245.6	67	1693	1654	15.91	24.4	29.5	35.1
59	1499	1457	10.80	107.0	133.1	155.0	68	1696	1657	10.71	34.6	44.0	50.9
60	1525	1483	16.32	80.2	94.4	107.0	69	1752	1714	15.87	17.5	23.6	28.4
61	1530	1488	15.97	61.2	75.1	87.1	70	1758	1720	10.69	27.8	35.3	40.4
62	1573	1532	10.74	73.3	88.7	101.9	71	1866	1830	6.35	24.1	31.1	36.5
63	1596	1556	15.94	34.6	42.1	49.7	72	1975	1941	6.33	13.3	18.7	23.5
64	1617	1577	6.00	112.8	141.6	167.9							
Series F: 0.49% CH_2O−1.98% O_2−Ar													
73	1436	1421	10.79	223.2	274.6	316.4	79	1619	1605	15.92	41.6	50.1	59.7
74	1457	1442	16.04	139.8	164.6	183.8	80	1625	1611	6.73	88.9	108.0	121.6
75	1470	1456	15.91	112.5	133.1	151.9	81	1631	1618	10.65	56.9	70.4	80.5
76	1499	1485	10.68	111.2	134.3	152.5	82	1662	1649	6.25	79.9	94.1	106.7
77	1567	1553	15.88	65.7	76.5	85.4	83	1671	1658	10.55	44.5	52.4	58.6
78	1578	1564	10.77	84.3	101.1	116.9							
Series G: 1.00% CH_2O−5.96% O_2−Ar													
84	1363	1334	10.76	257.5	309.5	342.9	92	1585	1559	15.70	31.4	38.7	45.5
85	1416	1388	16.15	140.2	169.4	189.3	93	1615	1589	10.61	31.8	43.5	52.3
86	1420	1392	10.78	142.7	178.4	207.6	94	1635	1609	15.72	29.7	35.8	39.9
87	1425	1397	16.08	100.1	125.6	152.1	95	1655	1630	6.20	42.5	51.1	57.8
88	1491	1464	6.75	161.6	192.7	222.4	96	1694	1669	6.49	43.6	54.6	63.4
89	1494	1467	10.78	85.0	104.7	120.6	97	1763	1739	10.74	19.1	22.3	25.0
90	1530	1503	15.94	48.3	58.6	66.5	98	1792	1768	6.35	18.9	26.9	32.8
91	1565	1539	10.75	55.3	66.4	75.7	99	1831	1808	10.50	8.0	10.6	13.3

[a] Temperature after complete decomposition of trioxane. [b] Total concentration after complete decomposition of trioxane.

Results and Discussion

Seven series of experiments with different initial compositions, from pure pyrolysis to fuel-lean oxidation, were used in the present study. The mixture compositions, experimental conditions, and obtained characteristic times for CO profiles are listed in Table 1. Typical absorption profiles collected in the pyrolysis and oxidation runs are shown in Figure 1.

As stated earlier, the source of formaldehyde in our experiments was trioxane. At temperatures above 1300 K the unimolecular decomposition of trioxane is very fast, with a half-lifetime below 0.5 μs.[23−25] Therefore, instantaneous decomposition of trioxane to three molecules of formaldehyde was assumed. The effect of this endothermic process is to lower the calculated postshock temperature, T_5, to a new value,

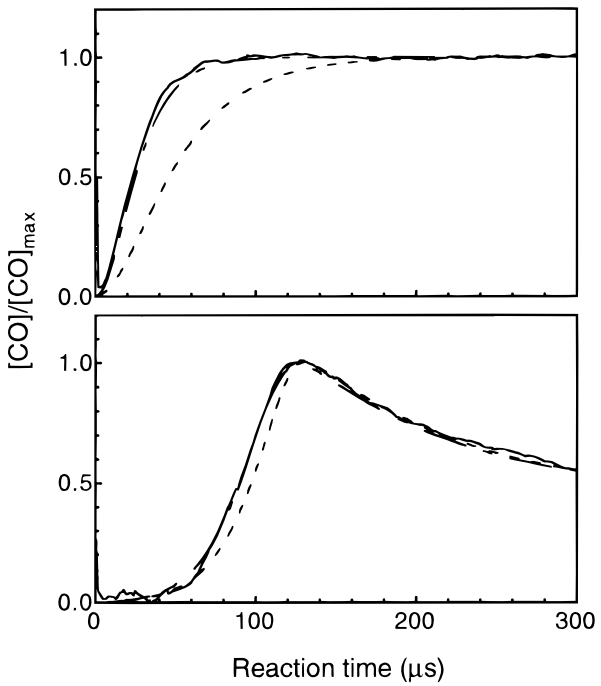

Figure 1. Typical CO profiles. Top panel: 1.97% CH_2O−Ar, T_0 = 1959 K, C_0 = 7.93 mol m^{-3}. Bottom panel: 1.5% CH_2O−1.5% O_2−Ar, T_0 = 1532 K, C_0 = 10.74 mol m^{-3}. (—) Experiment; (---) GRI-Mech 1.2; (− · −) present model.

designated as T_0—the initial temperature at which CH_2O chemistry begins. The computed values of T_0 and the corresponding total mixture density, C_0, are presented in Table 1. As can be seen, the reduction in temperature is at most 50 K. In these calculations we used the reported[23] enthalpy of formation for trioxane of −116 kcal/mol. The quoted uncertainty in the latter value is ±5 kcal/mol; this translates to a ±7 K temperature difference for a 1.5% CH_2O−Ar mixture, which is less than the uncertainty originating from the shock velocity measurements, ±15−20 K.

In an earlier shock-tube study, Buxton and Simpson[10] reported that CO formed in pyrolysis of CH_2O was vibrationally colder than expected according to the local Boltzmann distribution. Their observations, however, were made at significantly lower pressures and higher temperatures than ours. At the conditions employed here, no evidence of this phenomenon was seen in experimental traces. In addition, the estimated[10,26,27] ratio of CO relaxation time to half-rise time of CO profile for most of our conditions is below 0.06, which translates to an error of less than 2% in the determination of $t_{0.50}$. This level of error is rather small, compared to the rest of the experimental uncertainties, and therefore vibrational relaxation effects were neglected in the data analysis.

Kinetic information was deduced from the experimental data by matching the initial part of the CO profiles, from the onset of reaction up to the maximum in the absorption signal. Preliminary numerical analysis showed that the remaining part of the CO profiles (i.e., after the maximum) was mostly sensitive to the reaction CO + OH → H + CO_2 and hence did not provide additional information on formaldehyde reactions. Thus, each experimental profile was represented by three characteristic points, $t_{0.25}$, $t_{0.50}$, and $t_{0.75}$, the times at which the CO signal reached 0.25, 0.50, and 0.75 of its maximum value, respectively.

For numerical analysis each experimental series was represented by 4−6 sets of optimization targets $\{\tau_{0.25}, \tau_{0.50}, \tau_{0.75}\}$ chosen as follows. The experimental runs within each series were grouped according to the total concentration, C_0, usually into three groups with C_0 around 7, 11, and 16 mol m^{-3} (see Table 1). For each $C_0 \approx$ *constant* group, experimental characteristic times $t_{0.25}$, $t_{0.50}$, and $t_{0.75}$ were fitted into an Arrhenius-like form, as illustrated in Figure 2, and optimization targets τ were selected as representative points of these fits, typically two points near the ends of the temperature range. This procedure allowed us to smoothen experimental variations beforehand and hence to reduce the amount of numerical simulations required.

The kinetic modeling was based on a recent detailed reaction mechanism, GRI-Mech 1.2,[28] which includes formaldehyde reactions among its 177 elementary reactions of 32 chemical species. Sensitivity analysis indicated that, as typical, only a small number of rate constants have a meaningful effect on observable properties. Hence, only these rate parameters were adjusted, keeping the rest of the mechanism intact.

Determination of the rate parameter values was accomplished by numerical optimization using the method of solution mapping.[21,29−31] The objective function took the form

$$\Phi = \sum_{\text{all responses}} \sum_{i=0.25,0.50,0.75} \left(\frac{\tau_{i,\text{calculated}} - \tau_{i,\text{experimental}}}{\tau_{i,\text{experimental}}} \right)^2$$

with the optimization variables being the parameters A and θ of the modified Arrhenius rate coefficient expression $k = AT^n \exp(-\theta/T)$ and keeping n at the theoretically based values of GRI-Mech 1.2. The kinetic simulations were performed with CHEMKIN-II[32] and optimization with the IMSL routine ZXMWD.[33]

The initial calculations, using the unaltered GRI-Mech 1.2, predicted much slower pyrolysis of formaldehyde than was observed experimentally (Figure 1). A discussion of the discrepancies and plausible ways of their elimination is presented below.

Pyrolysis. The pyrolysis of formaldehyde at high temperatures, as suggested by past[7,9,10,12,13] and present studies, is primarily determined by the following set of reactions:

$$CH_2O + M \rightarrow H + HCO + M \quad (1a)$$

$$\rightarrow H_2 + CO + M \quad (1b)$$

$$H + CH_2O \rightarrow HCO + H_2 \quad (2)$$

$$HCO + M \rightarrow H + CO + M \quad (3)$$

$$H + HCO \rightarrow H_2 + CO \quad (4)$$

Sensitivity analysis revealed that under the conditions of the present shock-tube study the contribution of reaction 1b is negligible and the sensitivity to reactions 1a and 2 is substantially higher than to reactions 3 and 4 (Figure 3). In accord with the sensitivity analysis, numerical optimization showed that to reach agreement with the measured CO profiles, it was sufficient to vary just the rate coefficients of reactions 1a and 2. Inclusion of reactions 3 and 4 into the optimization, while producing only small changes in the final rate expressions for reactions 1a and 2, led to no significant improvement in the quality of fit to the experimental data. In light of these facts, we left the rate coefficients of reactions 1b, 3, and 4 at the GRI-Mech 1.2 expressions[28] and focused on those of reactions 1a and 2.

GRI-Mech 1.2 lists the rate coefficient expression of reaction 1a for the reverse direction, i.e., k_{-1a} rather than k_{1a}, with the

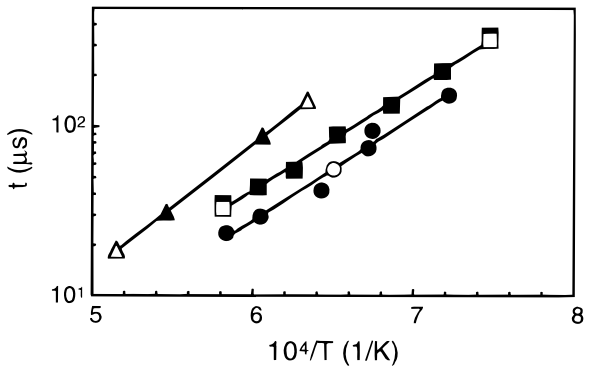

Figure 2. Illustration of selection of optimization targets. Filled symbols, experimental data points from series E, 1.5% CH_2O−1.50% O_2−Ar; open symbols, optimization targets. ▲, $C_0 \sim 6.25$ mol m^{-3}; ■, $C_0 \sim 10.75$ mol m^{-3}; ●, $C_0 \sim 16.0$ mol m^{-3}. Lines represent linear fits to experimental data.

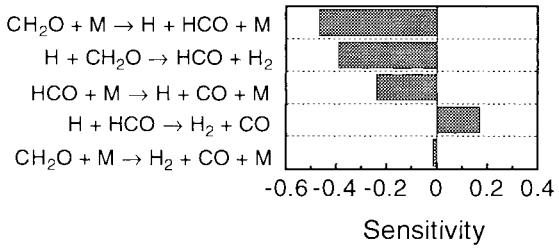

Figure 3. Logarithmic response sensitivities computed for formaldehyde pyrolysis. The displayed sensitivities refer to the half-rise time $t_{0.50}$ of CO signal calculated for a 1.97% CH_2O−Ar mixture at $T_0 =$ 1815 K and $C_0 = 10.7$ mol m^{-3} using GRI-Mech 1.2. Only values above 0.05 are shown, except for reaction −1b, $CH_2O + M \rightarrow H_2 + CO + M$, which is included for comparison.

latter calculated via the equilibrium constant. Thus, to be consistent, we varied k_{-1a} and used the thermochemistry of GRI-Mech 1.2 to calculate k_{1a}. We also note that the GRI-Mech rate expressions[28] are listed for N_2 bath gas. To obtain rate constants for Ar, as this study requires, the corresponding Arrhenius *A*-factor values were multiplied by the ratio of the collision efficiencies, β_{Ar}/β_{N_2}, fixed at the GRI-Mech 1.2 value[28] of 0.7 for reaction 1a. Selected literature recommendations[1,7,8,12,34,35] for the rate coefficients of reactions 1a and 2 are shown in Figure 4.

The optimization procedure found the rate coefficients of reactions 1a and 2 to be strongly correlated, as expected from the character of the sensitivity spectra—the two sensitivity coefficients are the largest ones and close to each other in value. The strong correlation manifests itself in the presence of a well-pronounced valley in the objective function, with steep walls and slowly changing height along the bottom path, as illustrated in Figure 5. Numerically, it implies that different pairs $\{k_{-1a}, k_2\}$ chosen along the valley provide fits of essentially the same quality. Stated differently, the present experimental data alone are insufficient to determine the two rate coefficients independently of one another.

To address this lack of uniqueness, one needs to include additional data into the joint optimization. However, it does not simply mean adding more experimental points, as increasing the number of data points from *similar* experimental responses, while possibly decreasing the random scatter, will not resolve the correlation.[31] Unfortunately, the present situation is typical of kinetic studies at high temperatures—it is essentially impossible to isolate an individual reaction among several occurring under such conditions, and experimental constraints limit determination of an adequate number of independent responses.

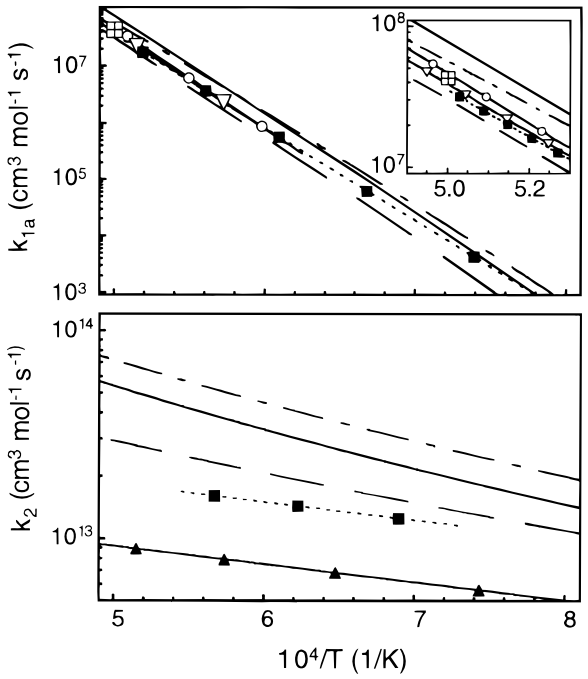

Figure 4. Selected literature recommendations for k_{1a} and k_2 in Ar bath gas. Top panel: reaction $CH_2O + M \rightarrow H + HCO + M$. Bottom panel: reaction $H + CH_2O \rightarrow HCO + H_2$. (−) present model; (− −) GRI-Mech 1.2; (■) Hidaka et al.;[12] (○) Dean et al.;[7] (⊞) Forst;[8] (− · −) Tsang and Hampson;[34] (▽) Rimpel and Just;[35] (▲) Warnatz.[1]

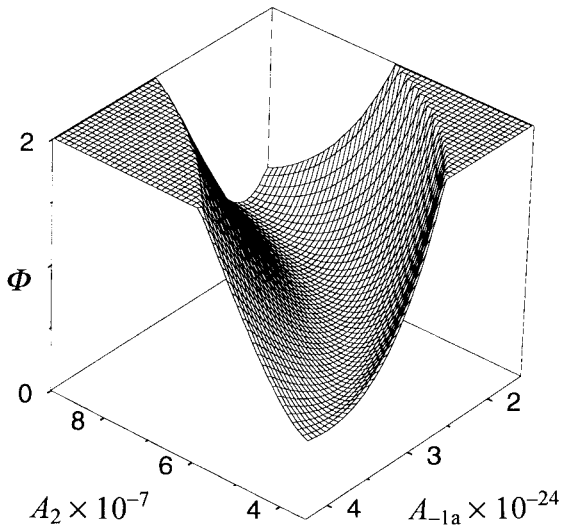

Figure 5. Illustration of the correlation between k_{-1a} and k_2. A_{-1a} and A_2 are the preexponential factors of $k_{-1a} = A_{-1a}T^{-2.57}e^{-215/T}$ and $k_2 = A_2T^{1.9}e^{-1380/T}$, respectively, and Φ is the objective function.

In the present study, we resolved the correlation between k_{-1a} and k_2 by assigning the latter a recent expression of Irdam et al.,[13]

$$k_2^{\mathrm{IKHW}} = 5.74 \times 10^7 T^{1.9} e^{-1380/T}\ \mathrm{cm^3\ mol^{-1}\ s^{-1}}$$

who derived it from tunneling-corrected transition-state-theory calculations for 250−5000 K and confirmed it by laser-schlieren shock tube experiments at 2200−3200 K. With k_2 fixed at this expression, parameter optimization performed with our pyrolysis data, collected over a temperature range of 1560−2270 K, resulted in (Table 2, case II)

$$k_{-1a}^{\mathrm{pyrolysis}} = 2.66 \times 10^{24} T^{-2.57} e^{-215/T}\ \mathrm{cm^6\ mol^{-2}\ s^{-1}}$$

TABLE 2: Results of Model Optimization

case	optimization variables[a] k_{-1a}	k_2	k_3	k_5	k_6	k_7	objective function Φ
			Pyrolysis Targets Only				
I	G	G	G				29.20
II	P	I	G				0.56
III	J	2.32 I	G				0.62
IV	J	1.87 I	0.54 G				0.60
			Joint Optimization				
V	G	G	G	G	G	G	41.30
VI	G	G	G	G	F	G	42.00
VII	P	I	G	G	G	G	4.74
VIII	P	I	G	G	F	G	5.52
IX	0.88 P	1.20 I	G	G	F	G	5.43
X	0.76 P	1.45 I	G	G	1.16 F	G	5.34
XI	1.07 P	1.27 I	0.70 G	0.50 G	1.45 F	0.50 G	4.45
XII	P	I	G	G	0.95 F	G	5.52
XIII	P	I	0.91 G	G	F	G	5.39
XIV	P	I	G	0.75 G	F	G	5.35
XV	P	I	G	G	F	1.20 G	5.43
XVI	1.11 P	I	0.87 G	G	F	G	5.31
XVII	P	I	0.90 G	G	F	0.95 G	5.39
XVIII	P	I	G	0.50 G	F	0.67 G	5.14
XIX	P	I	1.01 G	0.75 G	F	G	5.35
XX	P	I	0.88 G	0.50 G	F	0.51 G	5.05
XXI	P	I	0.89 G	0.50 G	1.46 F	0.97 G	4.94
XXII	1.27 P	I	0.70 G	0.50 G	1.34 F	0.53 G	4.55
XXIII	1.06 P	0.93 I	G	0.69 G	F	G	5.35
XXIV	J	1.85 I	G	G	F	G	6.58
XXV	J	2.32 I	G	0.50 G	1.38 F	0.50 G	5.15
XXVI	J	2.13 I	1.05 G	0.50 G	1.25 F	0.50 G	5.11

[a] Entry designations are P $= k_{-1a}^{\text{pyrolysis}}$, I $= k_2^{\text{IKHW}}$, $J = k_{1a}^{\text{RJ}} = 1.25 \times 10^{16}\ \text{e}^{-39171/T}\ \text{cm}^3\ \text{mol}^{-1}\ \text{s}^{-1}$ [the expression of Rimpel and Just (1989) as reported by Baulch et al.[35]], F $= k_6^{\text{fit}}$, and G represents the corresponding GRI-Mech 1.2 expression.[28] A letter listed alone indicates that the rate coefficient was fixed at the corresponding expression. A letter preceded by a number indicates that the preexponential factor of the corresponding expression was set free, and the number itself reports the multiplier obtained in optimization.

During this optimization, the power of T was fixed at the GRI-Mech value of -2.57, and the exponential coefficient was bounded by ± 1 kcal/mol from the GRI-Mech value of 1.4 kcal/mol. In all cases the exponential coefficient had a tendency to assume the lowest value. The rate coefficient obtained for reaction 1a is displayed graphically in Figure 4, where it is compared to selected literature data.

It should be kept in mind that our experimental data can be equally well fitted by other $\{k_{1a}, k_2\}$ pairs. For example, fixing k_{1a} at Rimpel and Just's expression[35] resulted in $k_2 = 2.32k_2^{\text{IKHW}}$ (Table 2, case III), substantially higher than other literature recommendations.[1,12,34,35]

The correlation between k_{-1a} and k_2 is visualized in Figure 5. The function depicted in Figure 5 is the least-squares residual computed with the rate coefficient temperature dependencies fixed, $k_{-1a} = A_{-1a}T^{-2.57}\text{e}^{-215/T}\ \text{cm}^6\ \text{mol}^{-2}\ \text{s}^{-1}$ and $k_2 = A_2T^{1.9}\text{e}^{-1380/T}\ \text{cm}^3\ \text{mol}^{-1}\ \text{s}^{-1}$, and varying only the preexponential factors A_{-1a} and A_2. The bottom line of the valley can be expressed as

$$A_{-1a} = 3.6 \times 10^{30} A_2^{-0.79}$$

The ability to identify and quantify such parameter correlations is an advantage of the numerical approach employed.

Oxidation. Sensitivity analysis shows that in addition to reactions 1−4, which govern the formaldehyde pyrolysis, the following CH_2O and HCO reactions become influential in the oxidative regimes of our shock-tube experiments:

$$O_2 + CH_2O \rightarrow HO_2 + HCO \quad (5)$$

$$HO_2 + CH_2O \rightarrow HCO + H_2O_2 \quad (6)$$

$$HCO + O_2 \rightarrow HO_2 + CO \quad (7)$$

$$O + CH_2O \rightarrow OH + HCO \quad (8)$$

$$OH + CH_2O \rightarrow HCO + H_2O \quad (9)$$

Figure 6 displays sensitivity spectra for all the oxidation mixtures studied. It lists reactions whose logarithmic response sensitivity (i.e., $\partial \ln \tau_{0.50}/\partial \ln k$) is above 0.05. Inspection of these results leads us to the following conclusions: (a) The sensitivity to the chain initiation, reaction 1a, is decreased dramatically compared to the pyrolysis case (cf. Figure 3). This implies that k_{1a} has to be determined predominantly by pyrolysis experiments. (b) The second decomposition channel of formaldehyde, reaction 1b, does not influence the oxidation rate at all. Therefore, its rate coefficient remained fixed at the GRI-Mech 1.2 expression.[28] (c) Reaction 2 has an appreciable sensitivity value. Nonetheless, leaving k_2 free did not help to resolve the correlation between k_{1a} and k_2. Hence, k_2 remained fixed at the expression of Irdam et al.[13] as in the pyrolysis case. (d) The sensitivities to reactions 4, 8, and 9 are relatively small, and therefore k_4, k_8, and k_9 were fixed at the GRI-Mech 1.2 expressions.[28] (e) Reactions 10−15 describe the part of hydrogen−oxygen chemistry that couples to the shock-tube oxidation of formaldehyde. Among them, reactions 11−15 do not exhibit measurable sensitivities. Reaction 10 does, but its rate coefficient is known with high accuracy.[36] Hence, k_{10} through k_{15} were fixed at the corresponding GRI-Mech 1.2 expressions[28] and not included into parameter optimization.

This left k_3, k_5, k_6, and k_7 as optimization variables for the oxidation part of the kinetic model. The dependence on k_2 and k_3 couples the oxidation model to the pyrolysis case, and the latter, in turn, determines k_{1a}. In light of this coupling, the minimized objective function Φ included both pyrolysis and oxidation targets.

The starting expressions of k_3, k_5, and k_7 were those of GRI-Mech 1.2,[28] and the starting expression of k_{-1a} was that determined from the pyrolysis experiments, $k_{-1a}^{\text{pyrolysis}}$. The rate coefficient of reaction 6 employed by GRI-Mech 1.2 is based on an older recommendation by Lloyd (1974);[37] hence, k_6 was refit using more recent experimental data.[18,19,38,39] The data points chosen for this purpose are listed in Table 3. Fixing the temperature exponent at 2.5, the midrange of Baulch et al.'s recommendation,[35] we obtained the following least-squares fit

$$k_6^{\text{fit}} = 4.11 \times 10^4 T^{2.5} \text{e}^{-5136/T}\ \text{cm}^3\ \text{mol}^{-1}\ \text{s}^{-1}$$

for the temperature range 540−1600 K. This expression along with the data points used in its derivation and the recent recommendation of Hochgreb and Dryer[18] are illustrated in Figure 7.

The results of several cases for the joint target optimization are displayed in Table 2. Only preexponential factors of the rate coefficients were set as free optimization variables, since we noticed in the initial phase of optimization that allowing changes in activation energies did not produce significant improvement in fitting the experimental data.

Case V in Table 2 is a reference case, using GRI-Mech 1.2 as is. In case VI, the rate coefficient of reaction 6 was replaced with the newly derived expression k_6^{fit}; this did not improve the quality of fit, as evidenced by the $\Phi_{\text{VI}} = 42.0$ value of the

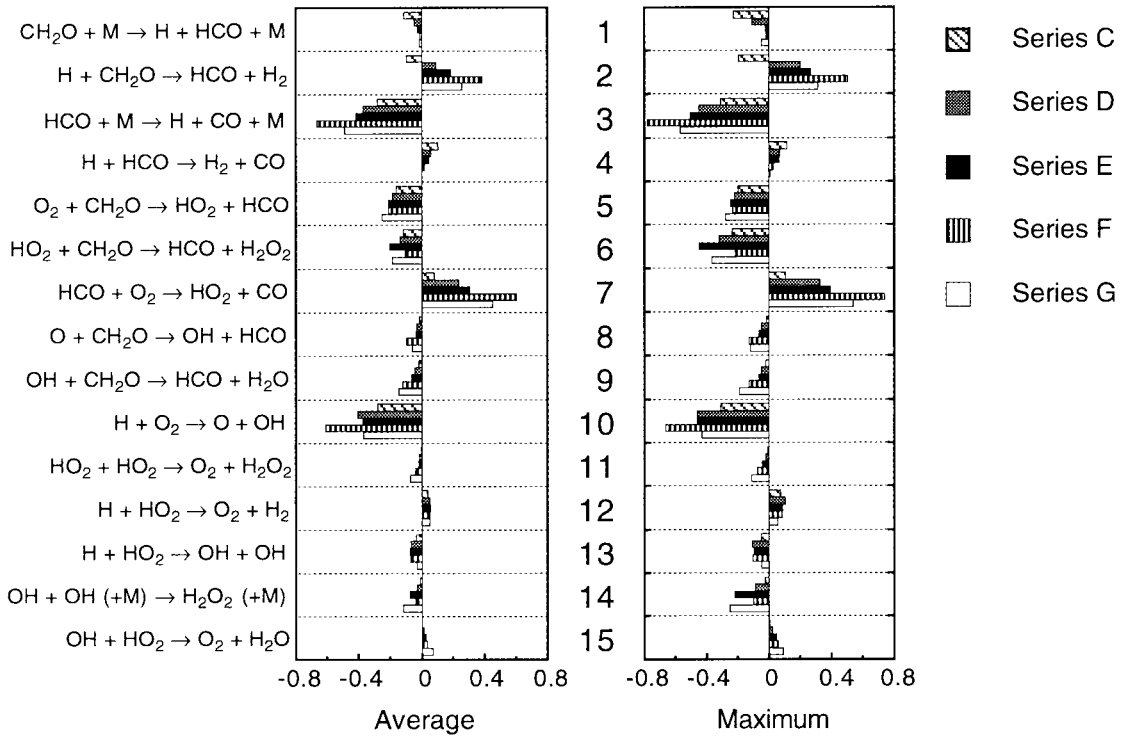

Figure 6. Logarithmic response sensitivities computed for formaldehyde oxidation using GRI-Mech 1.2. The displayed sensitivities refer to the half-rise time $t_{0.50}$ of the CO signal. Only values above 0.05 are shown. Average values are arithmetic means over all experimental runs in a series.

TABLE 3: Data Used in Derivation of k_6^{fit}

source	T (K)	k_6 (cm^3 mol^{-1} s^{-1})	statistical weight
Jemi-Alade et al. (1992)[a]	541	3.97×10^7	2/7
	592	9.39×10^7	2/7
	592	1.09×10^8	2/7
	616	1.02×10^8	2/7
	621	1.00×10^8	2/7
	624	1.25×10^8	2/7
	656	1.92×10^8	2/7
Baldwin and Walker (1979)[b]	773	5.50×10^8	2
Hochgreb and Dryer (1992)[c]	949	4.64×10^9	1
	1095	1.36×10^{10}	1
Hidaka et al. (1993)[d]	1256	5.66×10^{10}	1
	1600	2.58×10^{11}	1
this work[e]	1350	7.24×10^{10}	1
	1600	1.15×10^{11}	1

[a] Actual experimental measurements.[39] [b] Measured ratio $k_6/(k_{11})^{1/2} = 730$ cm$^{3/2}$ mol$^{-1/2}$ s$^{-1/2}$ at 773 K[38] multiplied by a more recent determination of $k_{11} = 5.46 \times 10^{11}$ cm^3 mol^{-1} s^{-1} at 773 K.[28,40] [c] The extreme temperature points for the recommended[18] expression $1.47 \times 10^{13} e^{-7650/T}$. [d] The extreme temperature points for the derived[19] expression $4.40 \times 10^6\ T^2\ e^{-6040/T}$. [e] Obtained by fitting the present pyrolysis and oxidation targets using GRI-Mech 1.2[28] with Lloyd's activation temperature[37] of 4025 K for k_6.

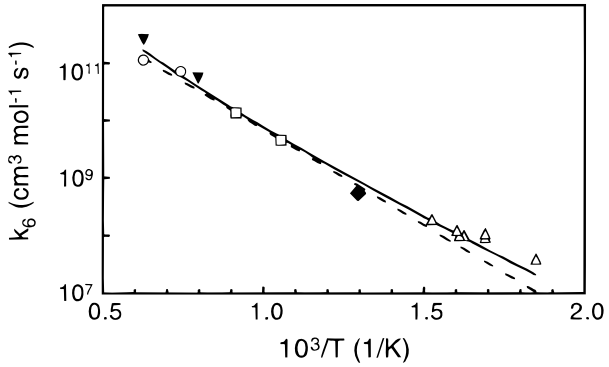

Figure 7. Arrhenius plot for rate coefficient k_6: (○) this work; (▼) Hidaka et al.;[19] (□) Hochgreb and Dryer;[18] (◆) modified data of Baldwin et al.;[38] (△) Jemi-Alade et al.;[39] (---) expression recommended by Hochgreb and Dryer;[18] (—) present recommendation, k_6^{fit}.

objective function compared to the baseline value $\Phi_V = 41.3$. A major improvement came with replacement of k_{-1a} and k_2 by the expressions determined from the pyrolysis data, namely $k_{-1a}^{pyrolysis}$ and k_2^{IKHW}. Regardless of whether we used GRI-Mech's expression or k_6^{fit} for reaction 6, the objective function drops by about a factor of 8 to $\Phi_{VII} = 4.74$ and $\Phi_{VIII} = 5.52$, respectively. (The lower Φ in case VII is due to the lower temperature dependence of the GRI-Mech 1.2 expression for k_6; however, the latter does not fit the low-temperature data[18,38,39] well.) The objective function remains at about the same level with all other possible modifications, as demonstrated by the rest of the optimization cases presented in Table 2. For instance, in cases IX and X the preexponential factors of k_{-1a} and k_2 are set free, but this results in only a minute reduction in the objective function. No optimization cases could resolve the correlation between k_{-1a} and k_2.

As expected, the objective function Φ attains the smallest value with all optimization variables set free, case XI in Table 2. In this case, k_3, k_5, and k_7 reach the lower boundaries of the corresponding variation domains, the latter based on existing theoretical and experimental literature data. Considering the scatter in the experimental data and the relatively small change in Φ, this behavior is indicative of a "random drift" rather than a definite trend. The value of $k_3^{GRI-Mech\ 1.2}$ is already at the lower boundary and $k_{-1a}^{pyrolysis}$ at the upper boundary of the majority of literature values, and hence further decrease of $k_3^{GRI-Mech\ 1.2}$ or further increase of $k_{-1a}^{pyrolysis}$ will produce larger departures from the consensus values.

Based on these considerations, our recommended rate coefficient set is that of case VIII. It combines a minimal number of rate parameter alterations with essentially the same quality of fit as the free optimization (case XI). The rate coefficient

TABLE 4: Summary of Rate Expressions

no.	reaction	k (cm^3, mol, s, K)	ref
−1a	$H + HCO + M \rightarrow CH_2O + M$	$2.66 \times 10^{24} T^{-2.57} e^{-215/T}$	this work
−1b	$H_2 + CO + M \rightarrow CH_2O + M$	$5.07 \times 10^{27} T^{-3.42} e^{-42450/T}$	28
2	$H + CH_2O \rightarrow HCO + H_2$	$5.74 \times 10^{7} T^{1.9} e^{-1380/T}$	13
3	$HCO + M \rightarrow H + CO + M$	$1.87 \times 10^{17} T^{-1} e^{-8560/T}$	28, 41
4	$H + HCO \rightarrow H_2 + CO$	7.34×10^{13}	28, 42
5	$O_2 + CH_2O \rightarrow HO_2 + HCO$	$1.0 \times 10^{14} e^{-20130/T}$	28, 43
6	$HO_2 + CH_2O \rightarrow HCO + H_2O_2$	$4.11 \times 10^{4} T^{2.5} e^{-5136/T}$	this work
7	$HCO + O_2 \rightarrow HO_2 + CO$	$7.60 \times 10^{12} e^{-200/T}$	28, 44
8	$O + CH_2O \rightarrow OH + HCO$	$3.90 \times 10^{13} e^{-1780/T}$	28
9	$OH + CH_2O \rightarrow HCO + H_2O$	$3.43 \times 10^{9} T^{1.18} e^{225/T}$	28, 34
10	$H + O_2 \rightarrow O + OH$	$8.30 \times 10^{13} e^{-7255/T}$	28, 36
11	$HO_2 + HO_2 \rightarrow H_2O_2 + O_2$	$1.30 \times 10^{11} e^{820/T} + 4.20 \times 10^{14} e^{-6040/T}$	28, 40
12	$H + HO_2 \rightarrow O_2 + H_2$	$2.80 \times 10^{13} e^{-537/T}$	28
13	$H + HO_2 \rightarrow OH + OH$	$1.34 \times 10^{14} e^{-320/T}$	28
14	$OH + OH + M \rightarrow H_2O_2 + M$	$2.30 \times 10^{18} T^{-0.9} e^{856/T}$	28
15	$OH + HO_2 \rightarrow O_2 + H_2O$	$2.90 \times 10^{13} e^{252/T}$	28, 45

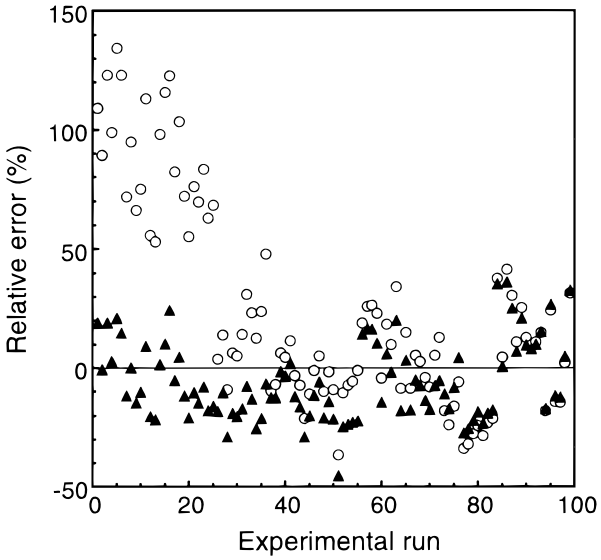

Figure 8. Relative errors obtained in numerical predictions of $t_{0.50}$. The horizontal axis refers to the experimental runs of Table 1. (○) GRI-Mech 1.2; (▲) present model.

of reaction 2 of the recommended set is kept at the literature expression,[13] and that of reaction 6 fits both the low-[18,38,39] and high-temperature[19] experiments, including the present ones, as evidenced by the results of optimization case XII.

The recommended rate parameter set is summarized in Table 4, and its prediction of our experimental profiles is illustrated in Figure 1. Figure 8 displays the relative errors obtained in numerical simulations of the present experimental measurements using GRI-Mech 1.2 and the new reaction model. As can be seen, the agreement produced by the new model is generally good, with one standard deviation 17%.

Validation. The reaction mechanism that contains the recommended reaction set (case VIII), referred to hereafter as the *present model*, was further tested against available literature data on high-temperature formaldehyde pyrolysis and oxidation. This section reports the results of the validation tests. All of the experimental studies listed below used paraformaldehyde as the source of CH_2O, whereas in the present study trioxane was used for this purpose.

Dean et al. determined apparent rate constants of formaldehyde decay during shock-tube pyrolysis[7] and oxidation[14] by measuring infrared emission of formaldehyde. A comparison

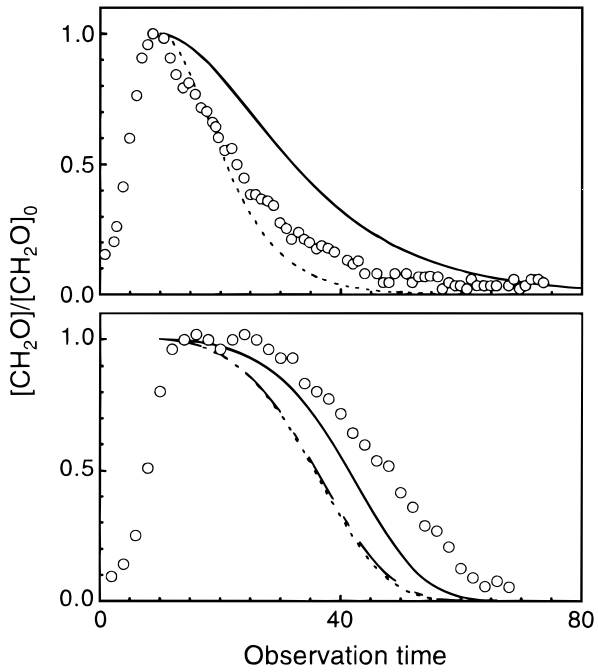

Figure 9. Comparison of model predictions with experimental data of Dean et al.[7,14] Offset time of 10 μs is included in the numerical simulations to account for shock passage over the observation window.[7,14] Top panel: 1.01% CH_2O−Ar, $T = 2150$ K, [M] = 7.4 mol m^{-3}. Bottom panel: 0.5% CH_2O−0.88% O_2−Ar, $T = 1935$ K, [M] = 6.8 mol m^{-3}. (○) experiment; (—) GRI-Mech 1.2; (---) present model (optimization case VIII); (— · —) optimization case XI.

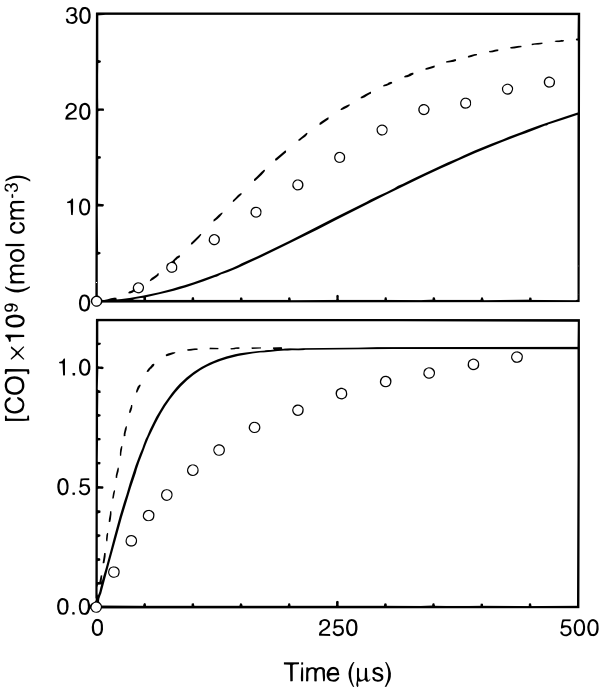

Figure 10. Comparison of model predictions with experimental data of Saito et al.[9] Top panel: 0.29% CH_2O−Ar, $T = 1725$ K, [M] = 9.8 mol m^{-3}. Bottom panel: 100 ppm CH_2O−Ar, $T = 2325$ K, [M] = 10.8 mol m^{-3}. (○) experiment; (—) GRI-Mech 1.2; (---) present model.

of their data with the numerical predictions of GRI-Mech 1.2 and the present model is presented in Figure 9. As can be seen, the pyrolysis data are predicted relatively well by the present model, closer than by GRI-Mech 1.2. At the same time, both models significantly overpredict the formaldehyde oxidation rate, GRI-Mech 1.2 being now closer to the experimental profile. Unfortunately, the numerical predictions are greatly affected by

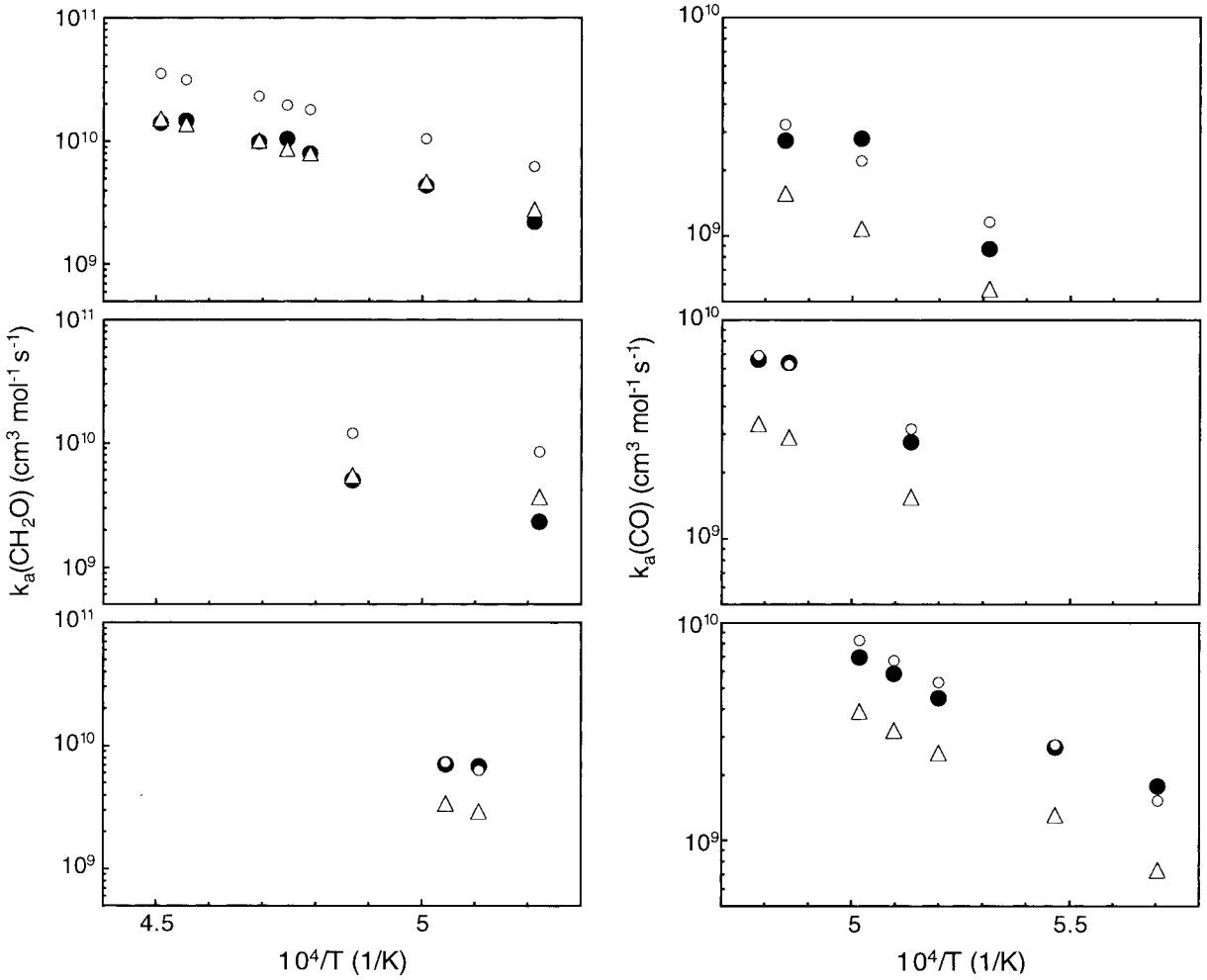

Figure 11. Comparison of model predictions with experimental data of Buxton and Simpson.[10] The panels on the left display apparent rate constant of CH_2O decay: top, ~ 2% CH_2O−Ar, [M] ~ 2.5 mol m^{-3}; middle, 1.0% CH_2O−Ar, [M] ~ 5 mol m^{-3}; and bottom, 0.9% CH_2O−Ar, [M] ~ 22 mol m^{-3}. The panels on the right display apparent rate constant of CO formation: top, 0.05% CH_2O−Ar, [M] ~ 21 mol m^{-3}; middle, 0.2% CH_2O−Ar, [M] ~ 9.2 mol m^{-3}; and bottom, 1.3% CH_2O−Ar, [M] ~ 4.5 mol m^{-3}. (●) experiment; (△) GRI-Mech 1.2; (○) present model.

the magnitude of the time offset introduced to account for the shock passage across the observation window.[7,14] The experimental $[CH_2O]/[CH_2O]_0$ ratio does not originate at 1, as should be the case, but at a value close to 0.1. This manifests a large uncertainty associated with the experiment itself, and in light of it, the agreement we obtained is acceptable.

Saito et al.[9] studied shock-tube pyrolysis of 50, 100, and 2900 ppm mixtures of CH_2O in Ar by infrared emission of CH_2O and CO and resonance absorption of H atoms. The temperature range studied extended from 1725 to 2640 K. The present model predicts the CO production measured for the 2900 ppm mixture reasonably well, but for the 50 and 100 ppm mixtures the experimental CO profiles rise 3−4 times more slowly than those calculated by GRI-Mech 1.2 and the present model (Figure 10). The problem, we believe, lies in the experiment.[9] We reached this conclusion by comparing experimental observations of Saito et al.[9] and Hidaka et al.[12] for the same mixture, 100 ppm CH_2O−Ar, examined by the two groups under similar conditions, at total concentrations of ~11 and ~16 mol m^{-3}, respectively. The half-lifetime of CH_2O reported by Hidaka et al.[12] for this mixture at 1907 K is 135 μs. The apparent activation energy of the CH_2O decay is about 50 kcal/mol, as reported by Dean et al.[7] and Buxton and Simpson.[10] Extrapolating the 135 μs value of Hidaka et al.[12] using the 50 kcal/mol experimental activation energy to 2325 K results in 15 μs. Saito et al.'s value[9] for this temperature is about 90 μs, i.e., a factor of 6 larger. By comparison, the GRI-Mech 1.2 prediction is 38 μs and that of the present model 21 μs, close to the extrapolated value of 15 μs. Another possible complication for the highly diluted mixtures, as indicated by our sensitivity calculations, is an increasing role of the molecular channel of formaldehyde decomposition, reaction 1b.

Buxton and Simpson[10] studied formaldehyde pyrolysis behind incident shock waves over a temperature range of 1750−2120 K by monitoring CH_2O and CO absorption with a CW CO laser. Comparison of our numerical predictions with their CH_2O absorption measurements is presented in the left panels of Figure 11. In the case of lower density mixtures, shown in the top and middle panels, the experimental data are predicted closely by GRI-Mech 1.2 but overestimated by about a factor of 2 by the present model. At higher densities, shown in the bottom panel, the situation is reversed: present model's predictions fall on the experimental points, but GRI-Mech 1.2 underpredicts them by a factor of 2. Close agreement of the present model with the experimental data is also observed for the CO absorption measurements, shown in the right panels of Figure 11. Buxton and Simpson[10] noted a difference between the CH_2O decay and CO production rates for similar mixtures (e.g., their observed rate constants for group 2 and 4, both investigated under almost identical conditions, differ by a factor 2; see Figure 1 of ref 10). The difference was attributed by them to a possible breakdown of the steady-state approximation used in their

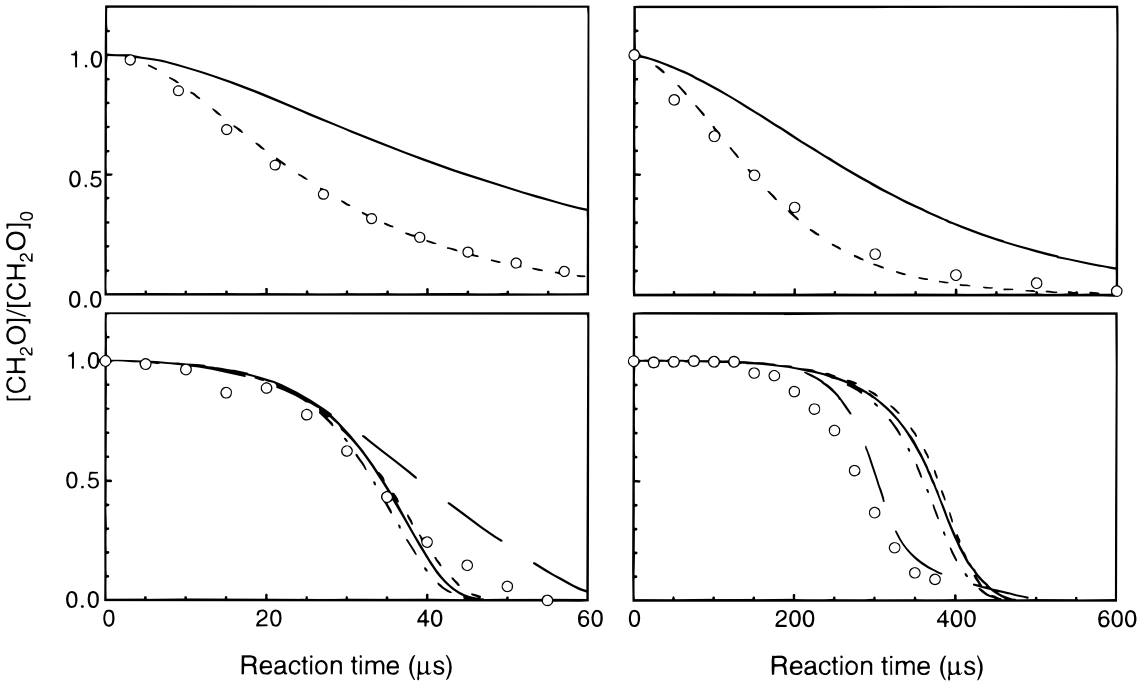

Figure 12. Comparison of model predictions with experimental data of Hidaka et al.[12,19] Top left panel: 4% CH_2O−Ar, $T = 1805$ K, [M] = 19.0 mol m^{-3}; top right panel: 0.01% CH_2O−Ar, $T = 1907$ K, [M] = 16.9 mol m^{-3}; bottom left panel: 1% CH_2O−4% O_2−Ar, $T = 1583$ K, [M] = 16.6 mol m^{-3}; bottom right panel: 4% CH_2O−1% O_2−Ar, $T = 1256$ K, [M] = 15.0 mol m^{-3}. (○) experiment (left panels, CH_2O absorption; right panels, CH_2O emission); (—) GRI-Mech 1.2; (---) present model (optimization case VIII); (— · —) optimization case XI; (— —) calculations of Hidaka et al.[19]

analysis. They also reported differing signal-to-noise (S/N) ratios: for CH_2O absorption S/N ∼ 5 whereas for CO absorption S/N > 25. This implies that CO measurements are more accurate, and the present model is in good agreement with these data.

The most recent experimental investigation of CH_2O pyrolysis and oxidation was carried out by Hidaka et al.,[12,19] who monitored infrared absorption and emission of CH_2O behind reflected shock waves in the temperature range 1160−1890 K. As with the CO absorption data of Buxton and Simpson,[10] the experimental rates of Hidaka et al. determined for pyrolysis (Figure 12, top panels) are almost twice as fast as those calculated with GRI-Mech 1.2. The agreement with the present model is excellent for both absorption (Figure 12, top left) and emission (Figure 12, top right) for the entire range of initial formaldehyde concentrations studied, namely, 4, 2, 1, 0.1, and 0.01% CH_2O in Ar. The agreement is also good for the oxidation cases (Figure 12, bottom left), except for a 4% CH_2O − 1% O_2−Ar mixture (Figure 12, bottom right). A sensitivity analysis showed that for this particular set of conditions reaction 6 is the most influential. It would take a 70% increase in k_6^{fit} to bring the model into agreement with these data. However, such a change deteriorates the quality of fit for our targets, increasing the value of the objective function from 5.52 (optimization case VIII) to 7.69.

Extrapolation of the rate expressions to lower temperatures allows a comparison of the present model with experimental data of Hochgreb and Dryer.[18] These authors investigated formaldehyde oxidation in an atmospheric-pressure flow reactor at temperatures around 1000 K. Species concentrations were obtained by gas chromatography of samples withdrawn from 15 axial locations along the reactor through a water-cooled probe. The present model is in close agreement with experimental traces at stoichiometric ratios of 0.013−1.56; a typical comparison is illustrated in Figure 13. For the very rich mixtures (stoichiometric ratios 30.6, 31.5, and 36.7) the agreement is poor, but Hochgreb and Dryer[18] also reported difficulties in fitting these data. In light of this, we consider the overall agreement as acceptable.

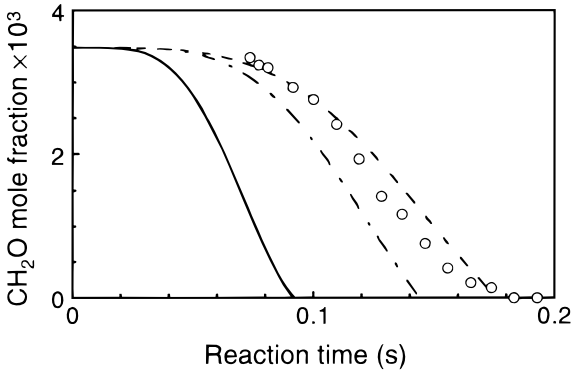

Figure 13. Comparison of model predictions with experimental data of Hochgreb and Dryer.[18] The offset time is 69.7 ms;[18] 3480 ppm CH_2O−2230 ppm O_2−Ar, $T = 945$ K, [M] = 12.9 mol m^{-3}. (○) experiment; (—) GRI-Mech 1.2; (---) present model (optimization case VIII); (— · —) optimization case XI.

Conclusions

The experimental data collected in the presented study were successfully modeled by modifying three rate coefficients of the GRI-Mech 1.2 set,[28] identified here as k_{1a}, k_2, and k_6. The analysis, performed by a systematic optimization, revealed a strong correlation between k_{1a} and k_2, indicating that information contained in the experimental data alone is not sufficient to determine a unique combination of k_{1a} and k_2. Assuming a recent expression for k_2, obtained in tunneling-corrected TST calculations of Irdam et al.,[13] produced a k_{1a} expression close to RRKM calculations of Tsang and Hampson.[34] For k_6 we developed a new expression by fitting the present and literature data.[18,19,38,39] With these modifications, the model provides good

agreement with our experimental data and an acceptable agreement with most literature experiments. The recommended rate parameter set is presented in Table 4.

Acknowledgment. The work was supported by the Gas Research Institute, Contract 5092-260-2454.

References and Notes

(1) Warnatz, J. In *Combustion Chemistry*; Gardiner, W. C., Jr., Ed.; Springer-Verlag: New York, 1984; p 197.
(2) Westbrook, C. K.; Dryer, F. L. *Prog. Energy Combust. Sci.* **1984**, *10*, 1.
(3) Peeters, J.; Mahnen, G. *Fourteenth Symposium (International) on Combustion*; The Combustion Institute: Pittsburgh, PA, 1973; p 133.
(4) Norton, T. S.; Dryer, F. L. *Combust. Sci. Technol.* **1989**, *63*, 107.
(5) Hernandez, O.; Rhomberg, L.; Hogan, K.; Siegel-Scott, C.; Lai, D.; Grindstaff, G.; Henry, M.; Cotruvo, J. A. *J. Hazard. Mater.* **1994**, *39*, 161.
(6) Barker, J. R.; Herstrom, A. A.; Tingey, D. T. *Water Air Soil Pollut.* **1996**, *86*, 71.
(7) Dean, A. M.; Craig, B. L.; Johnson, R. L.; Schultz, M. C.; Wang, E. E. *Seventeenth Symposium (International) on Combustion*; The Combustion Institute: Pittsburgh, PA, 1979; p 577.
(8) Forst, W. *J. Phys. Chem.* **1983**, *87*, 4489.
(9) Saito, K.; Kakumoto, T.; Nakanishi, Y.; Imamura, A. *J. Phys. Chem.* **1985**, *89*, 3109.
(10) Buxton, J. P.; Simpson, C. J. S. M. *Chem. Phys. Lett.* **1986**, *128*, 577.
(11) Choudhury, T. K.; Lin, M. C. *Combust. Sci. Technol.* **1989**, *64*, 19.
(12) Hidaka, Y.; Taniguchi, T.; Kamesawa, T.; Masaoka, H.; Inami, K.; Kawano, H. *Int. J. Chem. Kinet.* **1993**, *25*, 305.
(13) Irdam, E. A.; Kiefer, J. N.; Harding, L. B.; Wagner, A. F. *Int. J. Chem. Kinet.* **1993**, *25*, 285.
(14) Dean, A. M.; Johnson, R. L.; Steiner, D. C. *Combust. Flame* **1980**, *37*, 41.
(15) de Guertechin, L. O.; Vandooren, J.; Van Tiggelen, P. J. *Bull. Soc. Chim. Belg.* **1983**, *92*, 663.
(16) Vandooren, J.; de Guertechin, O. L.; van Tiggelen, P. J. *Combust. Flame* **1986**, *64*, 127.
(17) Bott, J. F.; Cohen, N. *Int. J. Chem. Kinet.* **1991**, *23*, 1075.
(18) Hochgreb, S.; Dryer, F. L. *Combust. Flame* **1992**, *91*, 257.
(19) Hidaka, Y.; Taniguchi, T.; Tanaka, H.; Kamesawa, T.; Inami, K.; Kawano, H. *Combust. Flame* **1993**, *92*, 365.
(20) Bozzelli, J. W.; Dean, A. M. *J. Phys. Chem.* **1993**, *97*, 4427.
(21) Yuan, T.; Wang, C.; Yu, C.-L.; Frenklach, M.; Rabinowitz, M. *J. Phys. Chem.* **1991**, *95*, 1258.
(22) Yu, C.-L.; Wang, C.; Frenklach, M. *J. Phys. Chem.* **1995**, *99*, 14377.
(23) Irdam, E. A.; Kiefer, J. H. *Chem. Phys. Lett.* **1990**, *166*, 491.
(24) Aldridge, H. K.; Liu, X.; Lin, M. C.; Melius, C. F. *Int. J. Chem. Kinet.* **1991**, *23*, 947.
(25) Hochgreb, S.; Dryer, F. L. *J. Phys. Chem.* **1992**, *96*, 295.
(26) von Rosenberg, C. W., Jr.; Bray, K. N. C.; Pratt, N. H. *Thirteenth Symposium (International) on Combustion*; The Combustion Institute: Pittsburgh, PA, 1971; p 89.
(27) Martin, J. P.; Buckingham, M. R.; Chenery, J. A.; Simpson, C. J. S. M. *Chem. Phys.* **1983**, *74*, 15.
(28) Frenklach, M.; Wang, H.; Goldenberg, M.; Smith, G. P.; Golden, D. M.; Bowman, C. T.; Hanson, R. K.; Gardiner, W. C.; Lissianski, V. Report GRI-95/0058, Gas Research Institute, Chicago, IL, 1995 (see also http://www.me.berkeley.edu/gri_mech/).
(29) Frenklach, M. In *Combustion Chemistry*; Gardiner, W. C., Jr., Ed.; Springer-Verlag: New York, 1984; p 423.
(30) Miller, D.; Frenklach, M. *Int. J. Chem. Kinet.* **1983**, *15*, 677.
(31) Frenklach, M.; Wang, H.; Rabinowitz, M. J. *Prog. Energy Combust. Sci.* **1992**, *18*, 47.
(32) Kee, R. J.; Rupley, F. M.; Miller, J. A. *Chemkin-II: A Fortran Chemical Kinetics Package for the Analysis of Gas-Phase Chemical Kinetics*; Report SAND89-8009B UC-706, Sandia National Laboratories: Livermore, CA, 1993.
(33) Rice, J. R. *Numerical Methods, Software, and Analysis: IMSL Reference Edition*; McGraw-Hill: New York, 1983.
(34) Tsang, W.; Hampson, R. F. *J. Phys. Chem. Ref. Data* **1986**, *15*, 1087.
(35) Baulch, D. L.; Cobos, C. J.; Cox, R. A.; Esser, C.; Frank, P.; Just, T.; Kerr, J. A.; Pilling, M. J.; Troe, J.; Walker, R. W.; Warnatz, J. *J. Phys. Chem. Ref. Data* **1992**, *21*, 411.
(36) Yu, C.-L.; Frenklach, M.; Masten, D. A.; Hanson, R. K.; Bowman, C. T. *J. Phys. Chem.* **1994**, *98*, 4770.
(37) Lloyd, A. C. *Int. J. Chem. Kinet.* **1974**, *6*, 169.
(38) Baldwin, R. R.; Walker, R. W. *Seventeenth Symposium (International) on Combustion*; The Combustion Institute: Pittsburgh, PA, 1979; p 525.
(39) Jemi-Alade, A. A.; Lightfoot, P. D.; Lesclaux, R. *Chem. Phys. Lett.* **1992**, *195*, 25.
(40) Hippler, H.; Troe, J.; Willner, J. *J. Chem. Phys.* **1990**, *93*, 1755.
(41) Timonen, R. S.; Ratajczak, E.; Gutman, D.; Wagner, A. F. *J. Phys. Chem.* **1987**, *91*, 5325.
(42) Timonen, R. S.; Ratajczak, E.; Gutman, D. *J. Phys. Chem.* **1987**, *91*, 692.
(43) Baldwin, R. R.; Walker, R. W. *Fourteenth Symposium (International) on Combustion*; The Combustion Institute: Pittsburgh, PA, 1973; p 241.
(44) Timonen, R. *Ann. Acad. Sci. Fenn., Ser. A2* **1988**, *218*, 3.
(45) Keyser, L. F. *J. Phys. Chem.* **1988**, *92*, 1193.